Available online at www.sciencedirect.com
ScienceDirect
International Journal of Solids and Structures 44 (2007) 7748–7766
INTERNATIONAL JOURNAL OF SOLIDS AND STRUCTURES
www.elsevier.com/locate/ijsolstr

Application of stress intensity to design of anisotropic/isotropic bi-materials with a wedge

Kum Cheol Shin [a], Won Seock Kim [b], Jung Ju Lee [b,*]

[a] *Advanced Technology Center, Corporate Research & Development Division, Hyundai-Kia Motors, 772-1, Jangduk-dong, Hwaseong-shi, Gyeonggi-do 445-706, South Korea*
[b] *Department of Mechanical Engineering, Korea Advanced Institute of Science and Technology, 373-1, Science Town, Daejeon 305-701, South Korea*

Received 28 December 2006; received in revised form 19 March 2007
Available online 23 May 2007

Abstract

Failure in anisotropic/isotropic bi-materials starts at the interface, and the interfacial failure is of interest to some engineering fields. However, since the procedure for evaluating stress intensities at the interface corner is very complicated and time-consuming, few researchers have used it to calculate singular stress fields and stress intensities, though doing so would allow prediction of the failure strength of a structure. In this paper, a simple procedure for obtaining stress intensities is introduced in the estimation of the failure strength of anisotropic/isotropic bi-materials. The expanded Stroh formalism is used to obtain asymptotic stress and displacement fields near the anisotropic/isotropic bi-material interface corner. The procedure makes it possible to calculate singular stress fields more easily than before. To evaluate stress intensities at the interface corner, a path-independent conservative line integral derived from Betti's reciprocal principle is used. To present a detailed description of the procedure, we describe the procedure of calculating singular stress fields and stress intensities of co-cured double lap joints with a wedge that consists of carbon fiber reinforced plastic composite and steel adherends.

We found two singular terms in describing stress and displacement fields near the wedge tip, and each of them referred to a different deformation mode: mode I and II. Therefore, we needed both mode I and II stress intensities to predict the joint failure. Failure surfaces and interfaces of double lap joints were investigated, and a fracture criterion on the $K_{\mathrm{I}}^{n} - K_{\mathrm{II}}^{n}$ plane is presented.

Keywords: Fracture Mechanics; Stress intensity factor; Asymptotic analysis; Conservation integrals; Anisotropic/isotropic bi-materials

1. Introduction

In some engineering fields, such as electronics and aerospace structures, it is important to consider bonded structures. Within the framework of mechanical design, failure starts at the interface corner between adher-

* Corresponding author. Tel.: +82 42 869 3033; fax: +82 42 869 3210.
E-mail address: leejungju@kaist.ac.kr (J.J. Lee).

0020-7683/$ - see front matter © 2007 Elsevier Ltd. All rights reserved.
doi:10.1016/j.ijsolstr.2007.05.014

ends where stresses concentrate. Although most engineers have used stress based approaches, studies dealing with stress intensities at the interface corner are regarded as providing a reliable tool for predicting the failure of bonded structures. Therefore, some researchers have tried to calculate stress intensities at the interface corner of bonded structures (Reedy and Guess, 1993, 1997; Akisanya and Fleck, 1997; Labossiere and Dunn, 1999).

In recent years, advanced anisotropic materials, such as fiber reinforced composite materials and silicon are used to improve structural efficiency of aerospace, vehicle, and electronic structures. However, since conventional metal alloys are still used in most industrial structures, it is inevitable to consider bonded structures of anisotropic/isotropic bi-materials. Generally, the structural efficiency of bonded structures depends on not structure itself but on joint strength. Therefore, it is important to analyze mechanical behavior at the interface corner of anisotropic/isotropic bi-materials with cracks or wedges.

Many engineers have studied the joint strength of anisotropic/isotropic bi-materials based on stress analysis (Adams, 1987; Tong, 1998). However, this approach has non-negligible limits; difficulty in representing the stress states at the interface corner tip, indispensable introduction of non-linear elasticity or plasticity for an accurate analysis, and a large amount of time for finite element analysis due to the use of fine meshes. These drawbacks have led many engineers to introduce a fracture mechanics approach using stress intensities as design parameters instead of stress components near the interface corner tip. The method using stress intensities is very useful in the analysis of bonded structures, because it does not consider a specific stress component near the interface corner tip as a parameter of a failure criterion. Instead it uses the amplitude of the singular stress field, the stress intensity. In addition, it is not necessary to consider the non-linear characteristics of the materials if the contour integral is performed at a distance somewhat removed from the interface corner tip. Moreover, it provides good results even if coarse meshes are used for finite element analysis. In this paper, we propose a method for obtaining stress intensities at the interface corner between anisotropic and isotropic adherends with a wedge to predict the failure strength of a bonded joint. In the following section of this chapter, we summarize relevant studies to this subject.

Muskhelishvili (1953) introduced a complex representation to make the general solution of the equations of the plane theory of elasticity simple, and Lekhnitskii (1963), Eshelby et al. (1953), and Stroh (1958) formulated the anisotropic elasticity problem. The Stroh formalism is very powerful for obtaining a solution of an anisotropic elasticity problem. Since the method was suggested by Stroh, it has been developed by many investigators. Basically, Stroh formalism provides a solution of an anisotropic elastic material, which means that it also provides that of an isotropic elastic material. However, the isotropic elasticity problem, which has three identical eigenvalues, is a special anisotropic elasticity problem. Ting (1996) gave a general solution of the isotropic elasticity problem using the anisotropic elasticity theory, but this solution yields very complicated results. Suo (1989, 1990) presented general solutions for both the isotropic bi-material problem and the anisotropic bi-material problem. Choi et al. (2003) applied the Stroh formalism to solve the anisotropic/isotropic elasticity problem with a crack. However, these researchers did not consider an anisotropic/isotropic bi-material problem with a wedge, which could be more complicated than the crack problem.

The procedure for obtaining stress intensities starts with evaluating the eigenvalues and the associated eigenvectors. Williams (1952, 1957) applied the eigenvector approach to a plate with notches, and he extended his work to a zero opening angle V-notch problem. England (1971) and Karp and Karal (1962) also put the eigenvector approach into practice for obtaining the eigenvalues of general opening notches. Dempsy and Sinclair (1979, 1981) and Dempsy (1981) gave equations that result in eigenvalues in a wide range of boundary and interface conditions. Ting and Chou (1981) and Ting (1982, 1986, 1996) solved some eigenvalue problems related to anisotropic materials. Stress singularity at bi-material wedges was also studied by many researchers. Bogy (1971) investigated the order of the singularity in the stress field at the bi-material isotropic wedge apex with various wedge angles and materials combinations. Chue and Liu (2002) did a similar job for the case of bi-material anisotropic wedges.

After obtaining the singular stress fields of anisotropic/isotropic bi-materials, the stress intensities at an interface corner tip with singular points, like crack or wedge tips, should be calculated to estimate possible failure at the points. The Reciprocal Work Contour Integral Method (RWCIM) is one of the most powerful

approaches for using finite element results to obtain stress intensities of configurations with cracks or wedges. This method does not need any special elements and relatively coarse element grids are sufficient to obtain good results. In addition, complex external boundaries and loading conditions can be easily handled. Hong and Stern (1978), Stern et al. (1976), Stern and Soni (1976), and Stern (1979) extended the RWCIM to yield stress intensities at the interface corner of isotropic bi-materials with zero opening cracks. Carpenter (1984), Carpenter and Byers (1987), Sinclair and Mullan (1982), Sinclair et al. (1984), and Sinclair (1985) applied this method to general opening crack problems. Labossiere and Dunn (1999) and Labossiere et al. (2002) applied the RWCIM to obtain stress intensities of cubic/isotropic bi-materials with notches.

In this investigation, the expanded Stroh formalism is introduced to obtain singular stress fields at the interface corner of anisotropic/isotropic bi-materials. The formalism is used to obtain eigenvalues and associated eigenvectors of anisotropic/isotropic bi-materials. Using the stress and displacement fields determined from the eigenvalues and eigenvectors, complimentary stress and displacement fields are also determined. Finally, stress intensities at the interface corner of anisotropic/isotropic bi-materials are explicitly presented using the RWCIM. To fully elucidate the proposed method, it is applied to a failure analysis of a co-cured double lap joint. In conclusion, a mixed-mode failure criterion is given, which allows estimation of a failure of an anisotropic/isotropic bi-material with a wedge.

2. Linear elasticity for two-dimensional deformation

For investigation of the behavior at the interface corner of bonded joints, consider the bi-material interface corner shown in Fig. 1. The upper and lower interface corner flanks are $\theta = \alpha$ and $\theta = -\beta$, where the angle θ is measured from the interface. The solid is composed of two materials, denoted by A and B, which are perfectly bonded along $\theta = 0$. A- and B-materials are anisotropic and isotropic materials, respectively. The interface corner flanks are traction-free, and the solid is loaded at remote boundaries by tractions or displacements.

Anisotropic elasticity, which enables us to describe the characteristics of the A-material in Fig. 1, is based on the Stroh formalism. Referring to a fixed rectangular coordinate system $x_i\,(i = 1,2,3)$, where σ_{ij}, u_i, and ε_{ij} are the stress, displacement, and strain, respectively, the general solution of the anisotropic adherend can be written as (Eshelby et al., 1953; Stroh, 1958)

$$\begin{aligned} \left\{\frac{\partial u_i}{\partial x_i}\right\} &= 2\mathrm{Re}[\mathbf{A}\mathbf{f}'(z)] \\ \{\sigma_{2i}\} &= 2\mathrm{Re}[\mathbf{B}\mathbf{f}'(z)] \\ \{\sigma_{1i}\} &= 2\mathrm{Re}[\mathbf{D}\mathbf{f}'(Z)]. \end{aligned} \tag{1}$$

In Eq. (1), $z = x_1 + px_2$. Basically, Stroh formalism deduces the solution by letting $\{u_i\} = 2\mathrm{Re}[\mathbf{A}\mathbf{f}(z)]$, where $\mathbf{f}(z) = [f_1(z_1), f_2(z_2), f_3(z_3)]^{\mathrm{T}}$. For the asymptotic analysis of the stress state near the bi-material interface corner, we assumed a solution form as $f(z) = \frac{1}{\lambda}z^{\lambda}\mathbf{q}$ to describe singular stress fields. $\mathbf{q}$ is a vector of constants to be

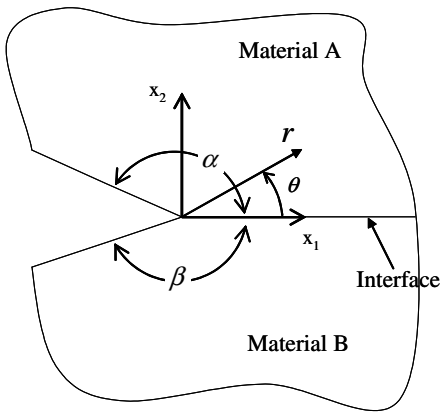

Fig. 1. General geometry of a bi-material interface corner.

determined. **A** is a matrix obtained from the eigenvalue problem of Eq. (2), the sextic equation, which gives six roots for the eigenvalue p and the corresponding eigenvector, **a**. Each column of A and each of p_i's are the eigenvector and the eigenvalue with positive imaginary part, respectively. Therefore **A** is a 3×3 complex matrix.

$$\left[\mathbf{C}_{i1k1} + p(\mathbf{C}_{i1k2} + \mathbf{C}_{i2k1}) + p^2\mathbf{C}_{i2k2}\right]\mathbf{a}_k = 0. \tag{2}$$

Matrices **B** and **D** can be calculated from $B_{ij} = \sum_{k=1}^{3}(C_{i2k1} + p_j C_{i2k2})A_{kj}$ and $D_{ij} = -B_{ij}p_j$ (not sum over j), respectively. For a more detailed procedure to obtain the solution, see Ting (1996).

In the case of isotropic elasticity, general solutions are given using the Muskhelishvili complex potentials (Muskhelishvili, 1953; Cho et al., 1994), as follows:

$$\begin{aligned}
&\sigma_{11} + \sigma_{22} = 2[\Phi(z) + \overline{\Phi(z)}]\\
&\sigma_{22} + \mathrm{i}\sigma_{12} = \overline{\Phi(z)} + \Omega(z) + (\bar{z} - z)\Phi'(z)\\
&\sigma_{32} + \sigma_{31} = \omega(z)\\
&-2iG\frac{\partial}{\partial x_1}(u_2 + \mathrm{i}u_1) = \kappa\overline{\Phi(z)} - \Omega(z) - (\bar{z} - z)\Phi'(z)\\
&\frac{\partial u_3}{\partial u_1} = \frac{1}{2Gi}[\omega(z) - \overline{\omega(z)}],
\end{aligned} \tag{3}$$

where $\kappa = 3 - 4\nu$ for plane strain and $\kappa = (3 - \nu)/(1 + \nu)$ for plane stress, ν and G are Poisson's ratio and shear modulus, respectively. $\Phi(z)$, $\Omega(z)$, and $\omega(z)$ are analytic functions of $z = x_1 + \mathrm{i}x_2$.

As we can see, the two formulations of elasticity problems are quite different which makes anisotropic/isotropic bi-material problems hard to be analyzed. Ting (1996) solved many elastic problems related to anisotropic bi-materials. And he mentioned that though isotropic materials are a special group of anisotropic materials, mathematically isotropic elasticity solution can not be deduced to isotropic elasticity solution easily. Recently, Choi et al. (2003) proposed the unified approach to anisotropic and isotropic elasticity for two-dimensional deformations under certain conditions. They had reconstructed the isotropic elasticity formulation, Eq. (3) into the frame work of the anisotropic elasticity, i.e., the Stroh formalism when the interface between dissimilar media lies along a straight line, usually set as x_1-axis. Here we utilize the expanded Stroh formalism to solve an anisotropic/isotropic bi-material wedge problem. Below are the rewritten formulations of isotropic elasticity (Choi et al., 2003).

$$\begin{aligned}
&\left\{\frac{\partial u_i}{\partial x_1}\right\} = 2\mathrm{Re}[\mathbf{A}^*\mathbf{g}'(z)]\\
&\{\sigma_{2i}\} = 2\mathrm{Re}[\mathbf{B}^*\mathbf{g}'(z)]\\
&\{\sigma_{1i}\} = 2\mathrm{Re}[\mathbf{D}^*\mathbf{g}'(z)],
\end{aligned} \tag{4}$$

where

$$\begin{aligned}
&\mathbf{g}'(z) = [\Phi(z), \Omega(z) + (\bar{z} - z)\Phi'(z), \omega(z)]^{\mathrm{T}} = \mathbf{f}^{*'}(z) + (\bar{z} - z)\mathbf{Q}^* \cdot \mathbf{f}^{*''}(z)\\
&\mathbf{f}^{*'}(z) = [\Phi(z), \Omega(z), \omega(z)]^{\mathrm{T}}\\
&\mathbf{A}^* = \frac{1}{4Gi}\begin{bmatrix}\kappa i & -i & 0\\ \kappa & 1 & 0\\ 0 & 0 & 2\end{bmatrix}, \quad \mathbf{B}^* = \frac{1}{2}\begin{bmatrix}i & -i & 0\\ 1 & 1 & 0\\ 0 & 0 & 1\end{bmatrix}, \quad \mathbf{D}^* = \frac{1}{2}\begin{bmatrix}3 & -1 & 0\\ i & -i & 0\\ 0 & 0 & -i\end{bmatrix}, \quad Q^* = \begin{bmatrix}0 & 0 & 0\\ 1 & 0 & 0\\ 0 & 0 & 0\end{bmatrix}.
\end{aligned} \tag{5}$$

The solution for the displacement was put to be $\{u_i\} = 2\mathrm{Re}[\mathbf{A}^*\mathbf{g}(z)]$, where $\mathbf{g}(z) = \mathbf{f}^*(z) + (\bar{z} - z)\mathbf{Q}^* \cdot \mathbf{f}^{*'}(z)$ to make the isotropic elasticity solution form similar to the anisotropic form. Arranging the general solution of the isotropic elasticity gives a new but identical solution with the original one. According to the equivalence theorem (Choi et al., 2003), the matrices $\mathbf{A}^*$, $\mathbf{B}^*$, $\mathbf{D}^*$, and $\mathbf{f}^*(z)$ for an isotropic material correspond, respectively, to **A**, **B**, **D**, and $\mathbf{f}(z)$ for an anisotropic material.

3. Stress singularity at an anisotropic/isotropic bimaterial wedge in bonded joints

Adhesively bonded lap joints are widely used as mechanical components in aerospace, vehicle, and electronic structures. A co-cured lap joint is one of the adhesively bonded lap joints in the concept of joining two dissimilar adherends using resin extracted from the uncured composite adherend. To help the reader comprehend the eigenvector approach to calculate eigenvalues and associated eigenvectors, we consider a wedge problem involved in anisotropic/isotropic co-cured double lap joint structure, as shown in Fig. 2. The wedge is composed of an anisotropic material with $\alpha = 180°$ and an isotropic material with $\beta = 90°$.

For a bi-material problem, boundary conditions are obtained by requiring displacement and traction continuity along the interface, i.e.,

$$\begin{aligned} &\mathbf{u}^{\mathrm{A}}(0) = \mathbf{u}^{\mathrm{B}}(0) \\ &\mathbf{t}^{\mathrm{A}}(0) = \mathbf{t}^{\mathrm{B}}(0). \end{aligned} \tag{6}$$

Applying Eq. (6), we obtain two tensor equations for calculating the stress singularity:

$$\begin{aligned} &\frac{1}{\lambda} r^{\lambda} \mathbf{A}^{\mathrm{A}} \mathbf{q}^{\mathrm{A}} + \frac{1}{\bar{\lambda}} r^{\bar{\lambda}} \overline{\mathbf{A}^{\mathrm{A}}} \overline{\mathbf{q}^{\mathrm{A}}} = \frac{1}{\lambda} r^{\lambda} \mathbf{A}^{\mathrm{B}} \mathbf{q}^{\mathrm{B}} + \frac{1}{\bar{\lambda}} r^{\bar{\lambda}} \overline{\mathbf{A}^{\mathrm{B}}} \overline{\mathbf{q}^{\mathrm{B}}} \\ &r^{\lambda-1} \mathbf{B}^{\mathrm{A}} \mathbf{q}^{\mathrm{A}} + r^{\bar{\lambda}-1} \overline{\mathbf{B}^{\mathrm{A}}} \overline{\mathbf{q}^{\mathrm{A}}} = r^{\lambda-1} \mathbf{B}^{\mathrm{B}} \mathbf{q}^{\mathrm{B}} + r^{\bar{\lambda}-1} \overline{\mathbf{B}^{\mathrm{B}}} \overline{\mathbf{q}^{\mathrm{B}}}. \end{aligned} \tag{7}$$

Imposing the traction-free requirement on the corner faces yields six homogenous boundary conditions as

$$\begin{aligned} &\mathbf{t}^{\mathrm{A}}(\pi) = 0 \\ &\mathbf{t}^{\mathrm{B}}\left(-\frac{\pi}{2}\right) = 0. \end{aligned} \tag{8}$$

Applying Eq. (8), we can obtain two tensor equations for calculating the stress singularity:

$$\begin{aligned} &r^{\lambda-1} \mathrm{e}^{\mathrm{i}\pi(\lambda-1)} \mathbf{B}^{\mathrm{A}} \mathbf{q}^{\mathrm{A}} + r^{\bar{\lambda}-1} \mathrm{e}^{-\mathrm{i}\pi(\bar{\lambda}-1)} \overline{\mathbf{B}^{\mathrm{A}}} \overline{\mathbf{q}^{\mathrm{A}}} = 0 \\ &r^{\lambda-1} \mathrm{e}^{-\frac{\pi \mathrm{i}}{2}(\lambda-1)} \mathbf{D}^{\mathrm{B}} \mathbf{V}^{\mathrm{B}} \mathbf{q}^{\mathrm{B}} + r^{\bar{\lambda}-1} \mathrm{e}^{\frac{\pi \mathrm{i}}{2}(\bar{\lambda}-1)} \overline{\mathbf{D}^{\mathrm{B}} \mathbf{V}^{\mathrm{B}}} \overline{\mathbf{q}^{\mathrm{B}}} = 0, \end{aligned} \tag{9}$$

where $\mathbf{V}^{\mathrm{B}} = \mathbf{I} - 2(\lambda - 1)\mathbf{Q}^{*}$. Applying these boundary conditions yields a set of simultaneous algebraic equations given by

$$\mathbf{K}(\lambda)\mathbf{q}(\lambda) = 0. \tag{10}$$

The vector $\mathbf{q}$ now contains the six components of the $\mathbf{q}$ vectors of materials A and B, i.e., $\mathbf{q} = [\mathbf{q}^{\mathrm{A}} \quad \mathbf{q}^{\mathrm{B}}]^{\mathrm{T}}$. Therefore, $\mathbf{K}(\lambda)$ takes the form

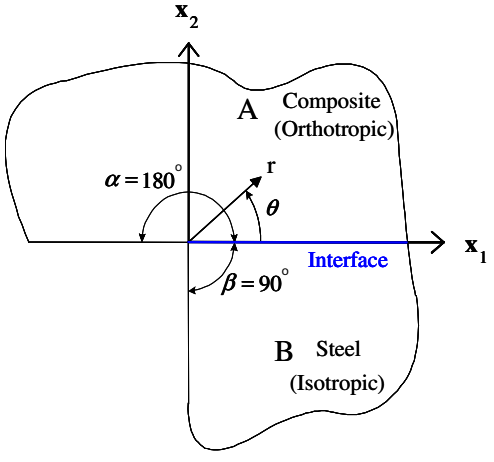

Fig. 2. Interface corner configuration of the anisotropic/isotropic double lap joint.

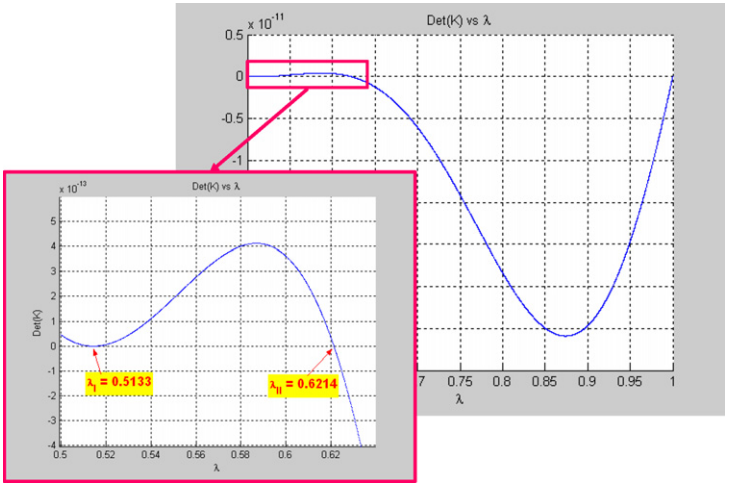

Fig. 3. Numerical solution of $\det[\mathbf{K}(\lambda)] = 0$ in the range of $0.5 < \mathrm{Re}[\lambda] < 1$.

$$\mathbf{K}(\lambda) = \begin{bmatrix} \frac{1}{\lambda}\mathbf{A}^{\mathrm{A}} - \frac{1}{\lambda}e^{i\pi(\lambda+\bar{\lambda})}\overline{\mathbf{A}^{\mathrm{A}}}\,\overline{\mathbf{B}^{\mathrm{A}^{-1}}}\mathbf{B}^{\mathrm{A}} & -\frac{1}{\lambda}\mathbf{A}^{\mathrm{B}} - \frac{1}{\lambda}e^{-\frac{\pi i}{2}(\lambda+\bar{\lambda})}\overline{\mathbf{A}^{\mathrm{B}}}\mathbf{U}^{\mathrm{B}} \\ \mathbf{B}^{\mathrm{A}} - e^{i\pi(\lambda+\bar{\lambda})}\mathbf{B}^{\mathrm{A}} & -\mathbf{B}^{\mathrm{B}} - e^{-\frac{\pi i}{2}(\lambda+\bar{\lambda})}\overline{\mathbf{B}^{\mathrm{B}}}\mathbf{U}^{\mathrm{B}} \end{bmatrix}, \tag{11}$$

where $\mathbf{U}^{\mathrm{B}} = \overline{\mathbf{V}^{\mathrm{B}^{-1}}\mathbf{D}^{\mathrm{B}^{-1}}}\mathbf{D}^{\mathrm{B}}\mathbf{V}^{\mathrm{B}}$. Here, $i = \sqrt{-1}$ and $()^{-1}$ stands for the inverse of the matrix. For a non-trivial solution we must have

$$\det[\mathbf{K}(\lambda)] = 0. \tag{12}$$

From Eq. (12), we can obtain the stress singularity order and the associated eigenvector $\mathbf{q}$. We found two roots of λ satisfying Eq. (12) within the range of $0 < \mathrm{Re}[\lambda] < 1$. Fig. 3 shows the function of $f(\lambda) = \det[\mathbf{K}(\lambda)]$, which intersects the abscissa twice in the range of $0.5 < \mathrm{Re}[\lambda] < 1$. The reason why we confine the range of λ to $0 < \mathrm{Re}[\lambda] < 1$ is to find singular stress terms without physical incompatibility. All components of the matrix $\mathbf{K}$ in Eq. (11) are composed of only elastic constants of the two adherends. The elastic properties of the two adherends, which consist of the co-cured double lap joint, are listed in Tables 1 and 2. The found eigenvalues were $\lambda_1 = 0.513$ and $\lambda_2 = 0.621$. Two eigenvalues mean that we need two singular terms in describing the stress and displacement fields near the wedge tip, as follows:

$$\begin{aligned} \sigma_{ij}^{\mathrm{M}} &= K_{\mathrm{I}}^{n} r^{\lambda_{\mathrm{I}}-1} f_{ij}^{\mathrm{IM}}(\theta) + K_{\mathrm{II}}^{n} r^{\lambda_{\mathrm{II}}-1} f_{ij}^{\mathrm{IIM}}(\theta) \\ u_{i}^{\mathrm{M}} &= K_{\mathrm{I}}^{n} r^{\lambda_{\mathrm{I}}} g_{i}^{\mathrm{IM}}(\theta) + K_{\mathrm{II}}^{n} r^{\lambda_{\mathrm{II}}} g_{i}^{\mathrm{IIM}}(\theta), \end{aligned} \tag{13}$$

where the superscript M becomes material-A for the upper adherend ($\theta \geqslant 0$) and material-B for the lower adherend ($\theta \leqslant 0$). The two-term expansion of the stress state is analogous to the classical mode I and II fields in the homogeneous crack or notch problem. However, in this interface corner problem, due to the material mismatch, modes I and II are neither symmetric nor antisymmetric with respect to the interface bisector. The subscripts and superscripts of I and II denote the first and second terms describing the singular stress fields, and they represent deformation modes but not the meaning of the opening and sliding modes, respectively, as in a homogeneous solid.

4. Asymptotic singular fields

Once the eigenvalue, λ, and the corresponding eigenvector, $\mathbf{q}$, are acquired, we can determine stress and displacement fields near the interface corner tip by applying the Stroh formalism and the expanded Stroh formalism to the two adherends, respectively. The angular variation functions of stress and displacement fields at the singularity dominated zone, $f_{ij}(\theta)$ and $g_i(\theta)$ in Eq. (13) can be expressed as:

Table 1
Material properties of the carbon fiber-epoxy composite material

Elastic properties	
E_1 (GPa)	131.6
$E_2 = E_3$ (GPa)	8.2
G_{12} (GPa)	4.5
ν_{12}	0.28
Coefficient of thermal expansion	
α_1 (10^{-6}/°C)	−0.9
$\alpha_2 = \alpha_3$ (10^{-6}/°C)	27
Thickness of a ply	
t (mm)	0.14

Table 2
Mechanical properties of the steel (SM45C)

Elastic properties	
E (GPa)	200
ν_{12}	0.3
Coefficient of thermal expansion	
α (10^{-6}/°C)	12

$$
\begin{aligned}
f_{1i}^{\mathrm{IA}}(\theta) &= \mathbf{D}^{\mathrm{A}}\mathrm{diag}[\zeta_\alpha^{\mathrm{A}}(\theta)^{\lambda_{\mathrm{I}}-1}]\mathbf{q}^{\mathrm{A^I}} + \overline{\mathbf{D}^{\mathrm{A}}}\mathrm{diag}[\overline{\zeta_\alpha^{\mathrm{A}}(\theta)^{\lambda_{\mathrm{I}}-1}}]\overline{\mathbf{q}^{\mathrm{A^I}}}\\
f_{2i}^{\mathrm{IA}}(\theta) &= \mathbf{B}^{\mathrm{A}}\mathrm{diag}[\zeta_\alpha^{\mathrm{A}}(\theta)^{\lambda_{\mathrm{I}}-1}]\mathbf{q}^{\mathrm{A^I}} + \overline{\mathbf{B}^{\mathrm{A}}}\mathrm{diag}[\overline{\zeta_\alpha^{\mathrm{A}}(\theta)^{\lambda_{\mathrm{I}}-1}}]\overline{\mathbf{q}^{\mathrm{A^I}}}\\
g_i^{\mathrm{IA}}(\theta) &= \frac{1}{\lambda_{\mathrm{I}}}\mathbf{A}^{\mathrm{A}}\mathrm{diag}[\zeta_\alpha^{\mathrm{A}}(\theta)^{\lambda_{\mathrm{I}}}]\mathbf{q}^{\mathrm{A^I}} + \frac{1}{\overline{\lambda_{\mathrm{I}}}}\overline{\mathbf{A}^{\mathrm{A}}}\mathrm{diag}\left[\overline{\zeta_\alpha^{\mathrm{A}}(\theta)^{\lambda_{\mathrm{II}}}}\right]\overline{\mathbf{q}^{\mathrm{A^I}}}\\
f_i^{\mathrm{IIA}}(\theta) &= \mathbf{D}^{\mathrm{A}}\mathrm{diag}[\zeta_\alpha^{\mathrm{A}}(\theta)^{\lambda_{\mathrm{II}}-1}]\mathbf{q}^{\mathrm{A^{II}}} + \overline{\mathbf{D}^{\mathrm{A}}}\mathrm{diag}[\overline{\zeta_\alpha^{\mathrm{A}}(\theta)^{\lambda_{\mathrm{II}}-1}}]\overline{\mathbf{q}^{\mathrm{A^{II}}}}\\
f_{2i}^{\mathrm{IIA}}(\theta) &= \mathbf{B}^{\mathrm{A}}\mathrm{diag}[\zeta_\alpha^{\mathrm{A}}(\theta)^{\lambda_{\mathrm{II}}-1}]\mathbf{q}^{\mathrm{A^{II}}} + \overline{\mathbf{B}^{\mathrm{A}}}\mathrm{diag}[\overline{\zeta_\alpha^{\mathrm{A}}(\theta)^{\lambda_{\mathrm{II}}-1}}]\overline{\mathbf{q}^{\mathrm{A^{II}}}}\\
g_i^{\mathrm{IIA}}(\theta) &= \frac{1}{\lambda_{\mathrm{II}}}\mathbf{A}^{\mathrm{A}}\mathrm{diag}[\zeta_\alpha^{\mathrm{A}}(\theta)^{\lambda_{\mathrm{II}}}]\mathbf{q}^{\mathrm{A^{II}}} + \frac{1}{\overline{\lambda_{\mathrm{II}}}}\overline{\mathbf{A}^{\mathrm{A}}}\mathrm{diag}\left[\overline{\zeta_\alpha^{\mathrm{A}}(\theta)^{\lambda_{\mathrm{II}}}}\right]\overline{\mathbf{q}^{\mathrm{A^{II}}}}\\
f_{1i}^{\mathrm{IB}}(\theta) &= \mathrm{e}^{\mathrm{i}\theta(\lambda_{\mathrm{I}}-1)}\mathbf{D}^{\mathrm{B}}[\mathbf{I} - (\lambda_{\mathrm{I}}-1)(1-\mathrm{e}^{-2\mathrm{i}\theta})\mathbf{Q}^*]\mathbf{q}^{\mathrm{B^I}} + \mathrm{e}^{-\mathrm{i}\theta(\overline{\lambda_{\mathrm{I}}}-1)}\overline{\mathbf{D}^{\mathrm{B}}}[\mathbf{I} - (\overline{\lambda_{\mathrm{I}}}-1)(1-\mathrm{e}^{2\mathrm{i}\theta})\mathbf{Q}^*]\overline{\mathbf{q}^{\mathrm{B^I}}}\\
f_{2i}^{\mathrm{IB}}(\theta) &= \mathrm{e}^{\mathrm{i}\theta(\lambda_{\mathrm{I}}-1)}\mathbf{B}^{\mathrm{B}}[\mathbf{I} - (\lambda_{\mathrm{I}}-1)(1-\mathrm{e}^{-2\mathrm{i}\theta})\mathbf{Q}^*]\mathbf{q}^{\mathrm{B^I}} + \mathrm{e}^{-\mathrm{i}\theta(\overline{\lambda_{\mathrm{I}}}-1)}\overline{\mathbf{B}^{\mathrm{B}}}[\mathbf{I} - (\overline{\lambda_{\mathrm{I}}}-1)(1-\mathrm{e}^{2\mathrm{i}\theta})\mathbf{Q}^*]\overline{\mathbf{q}^{\mathrm{B^I}}}\\
g_i^{\mathrm{IB}}(\theta) &= \mathrm{e}^{\mathrm{i}\theta\lambda_{\mathrm{I}}}\mathbf{A}^{\mathrm{B}}\left[\frac{1}{\lambda_1}\mathbf{I} - (1-\mathrm{e}^{-2\mathrm{i}\theta})\mathbf{Q}^*\right]\mathbf{q}^{\mathrm{B^I}} + \mathrm{e}^{-\mathrm{i}\theta\overline{\lambda_{\mathrm{I}}}}\overline{\mathbf{A}^{\mathrm{B}}}\left[\frac{1}{\overline{\lambda_{\mathrm{I}}}}\mathbf{I} - (1-\mathrm{e}^{2\mathrm{i}\theta})\mathbf{Q}^*\right]\overline{\mathbf{q}^{\mathrm{BI}}}\\
f_{1i}^{\mathrm{IIB}}(\theta) &= \mathrm{e}^{\mathrm{i}\theta(\lambda_{\mathrm{II}}-1)}\mathbf{D}^{\mathrm{B}}[\mathbf{I} - (\lambda_{\mathrm{II}}-1)(1-\mathrm{e}^{-2\mathrm{i}\theta})\mathbf{Q}^*]\mathbf{q}^{\mathrm{B^{II}}} + \mathrm{e}^{\mathrm{i}\theta(\overline{\lambda_{\mathrm{II}}}-1)}\overline{\mathbf{D}^{\mathrm{B}}}[\mathbf{I} - (\overline{\lambda_{\mathrm{II}}}-1)(1-\mathrm{e}^{2\mathrm{i}\theta})\mathbf{Q}^*]\overline{\mathbf{q}^{\mathrm{B^{II}}}}\\
f_{2i}^{\mathrm{IIB}}(\theta) &= \mathrm{e}^{\mathrm{i}\theta(\lambda_{\mathrm{II}}-1)}\mathbf{B}^{\mathrm{B}}[\mathbf{I} - (\lambda_{\mathrm{II}}-1)(1-\mathrm{e}^{-2\mathrm{i}\theta})\mathbf{Q}^*]\mathbf{q}^{\mathrm{B^{II}}} + \mathrm{e}^{-\mathrm{i}\theta(\overline{\lambda_{\mathrm{II}}}-1)}\overline{\mathbf{B}^{\mathrm{B}}}[\mathbf{I} - (\overline{\lambda_{\mathrm{II}}}-1)(1-\mathrm{e}^{2\mathrm{i}\theta})\mathbf{Q}^*]\overline{\mathbf{q}^{\mathrm{B^{II}}}}\\
g_i^{\mathrm{IIB}}(\theta) &= \mathrm{e}^{\mathrm{i}\theta\lambda_{\mathrm{II}}}\mathbf{A}^{\mathrm{B}}\left[\frac{1}{\lambda_{\mathrm{II}}}\mathbf{I} - (1-\mathrm{e}^{-2\mathrm{i}\theta})\mathbf{Q}^*\right]\mathbf{q}^{\mathrm{B^{II}}} + \mathrm{e}^{-\mathrm{i}\theta\overline{\lambda_{\mathrm{II}}}}\overline{\mathbf{A}^{\mathrm{B}}}\left[\frac{1}{\overline{\lambda_{\mathrm{II}}}}\mathbf{I} - (1-\mathrm{e}^{2\mathrm{i}\theta})\mathbf{Q}^*\right]\overline{\mathbf{q}^{\mathrm{B^{II}}}}.
\end{aligned}
\tag{14}
$$

Since the eigenvectors for each mode are determined only up to an arbitrary constant, we normalize the mode I fields as $f_{22}^{\mathrm{I}}(0) = 1$ so that $\sigma_{22}(\theta = 0) = K_{\mathrm{I}}^n r^{\lambda_{\mathrm{I}}-1}$ and the mode II fields as $f_{12}^{\mathrm{II}}(0) = -1$ so that $\sigma_{12}(\theta = 0) = K_{\mathrm{II}}^n r^{\lambda_{\mathrm{II}}-1}$. The same normalization is also applied to complementary stress fields which will be explained later. With this normalization, stress intensities can be scaled in a unified way.

Angular variation functions of stress and displacement, i.e., $f_{ij}(\theta)$ and $g_i(\theta)$ in the region dominated by stress singularity are shown in Figs. 4 and 6, respectively. Mode I and II stress variations show a similar trace of curves, while Mode I and II displacement variations show significant discrepancy. Figs. 5 and 7 show angular variations of stress and displacement fields, respectively, at the distance of 180 μm radius, obtained from finite

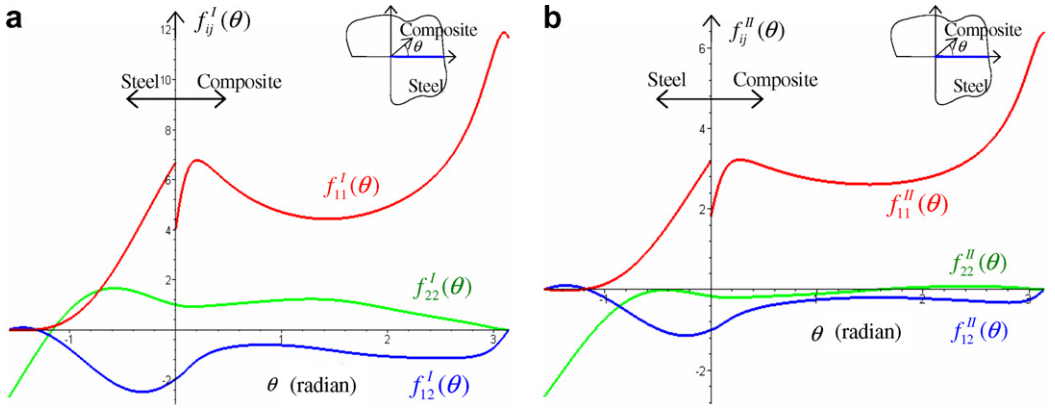

Fig. 4. Normalized angular variations of stress fields obtained from asymptotic analysis: (a) for mode I, (b) for mode II.

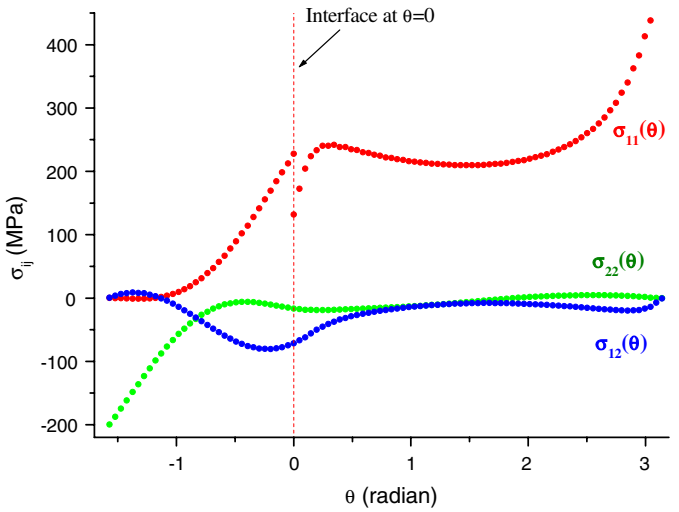

Fig. 5. Angular variations of stress fields obtained from FEM.

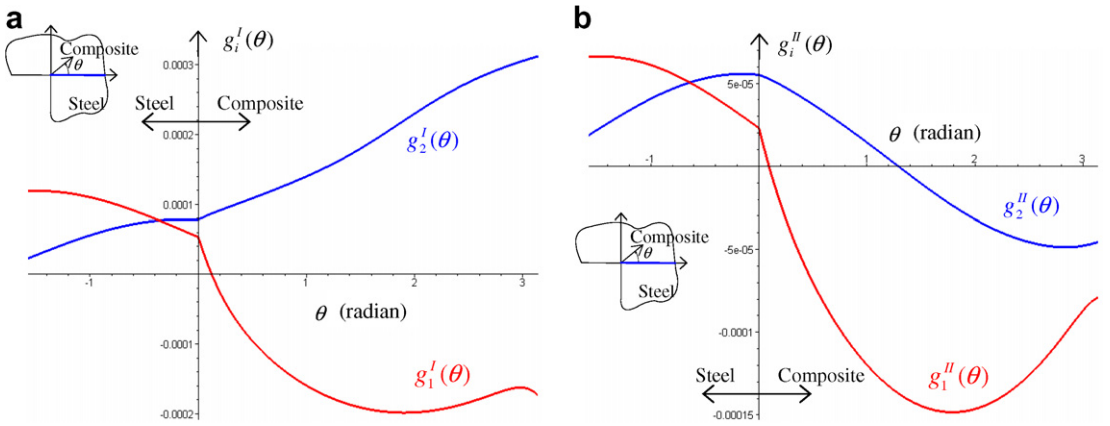

Fig. 6. Normalized angular variations of displacement fields obtained from asymptotic analysis: (a) for mode I, (b) for mode II.

element analysis of the co-cured double lap joint. Detail procedure of the finite element analysis is presented in chapter 6. We can see that angular variations of stress fields obtained from the finite element analysis are in good agreement with asymptotic solutions. In addition, displacement fields from the finite element analysis are

similar to the mode II asymptotic displacement fields. This means that the interface corner of the double lap joint specimen under tensile loading is liable to the mode II state more severely than the mode I state. As mentioned earlier, the Mode I and II fields do not show a symmetric or antisymmetric manner. Moreover, they are not opening or sliding modes as in a homogeneous crack or notch problem. The two modes, however, can be analogies of opening and sliding modes, because, for the bi-material mode I condition (the first singular term), interfacial normal stresses develop significantly, i.e., $f_{22}^{\mathrm{I}}(0) > 0$, while for the bi-material mode II condition (the second singular term), interfacial normal stresses become negligible and have a negative sign, i.e., $f_{22}^{\mathrm{II}}(0) < 0$.

The only quantities in Eq. (13) that are not obtained from the asymptotic analysis are the mode I and II stress intensities, K_{I}^{n} and K_{II}^{n}, which depend on a specific far-field geometry and loading conditions. These stress intensities will be determined in chapter 7, using a path-independent H-contour integral.

5. Experimental results

Fig. 8 shows a composite/steel double lap joint specimen used in this study. The materials comprising the specimen are steel and carbon fiber reinforced epoxy composite material. The carbon fiber-epoxy composite prepreg (USN150) is manufactured by SK Chemicals (Korea), and its mechanical properties are listed in Table 1. The stacking sequence of all specimens is $[0]_{16}$. Co-cured double lap joint specimens were fabricated under the manufacturer's recommended cure cycle for the composite material and were tested under the tensile loading condition. Fig. 9 illustrates the fabrication process of the co-cured joint. The shape and dimensions of the specimen are shown in Fig. 10 and are based on ASTM D3528-96 (2002).

Fig. 11 shows the tensile test apparatus and a fractured double lap joint specimen. The load-displacement response curve obtained from the tensile test is linear until an abrupt rupture, as shown in Fig. 12. This means that the co-cure bonded double lap joint shows brittle fracture behavior. Rupture occurs without any noticeable change in the rate of elongation. Additionally there is no difference between the ultimate strength and the

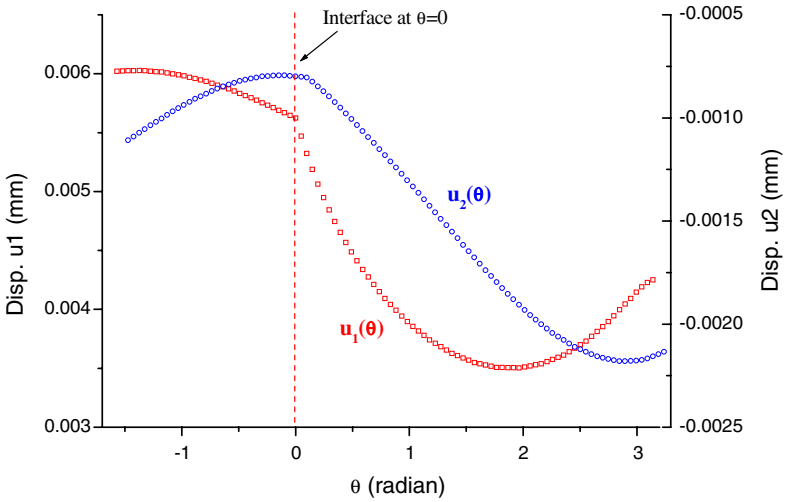

Fig. 7. Angular variations of displacement fields obtained from FEM.

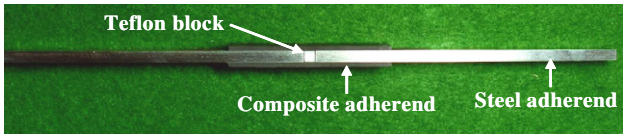

Fig. 8. Photograph of the co-cured double lap joint specimen.

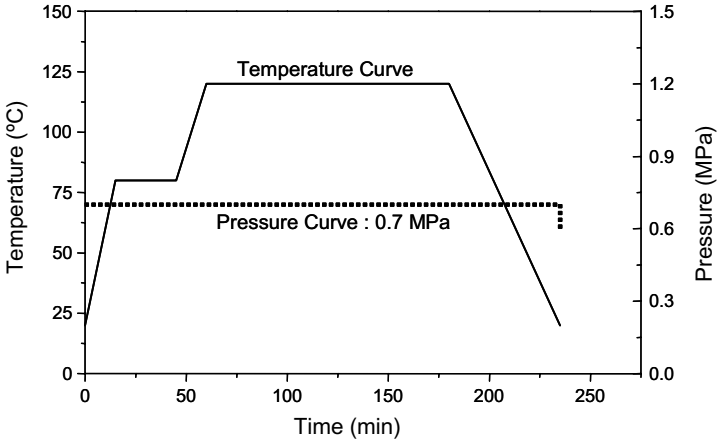

Fig. 9. Cure cycle of the composite material.

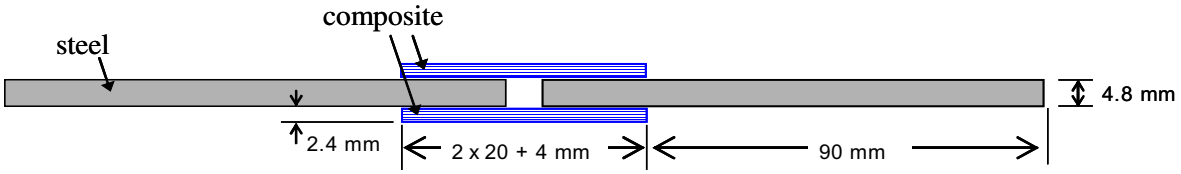

Fig. 10. Dimensions of the double lap joint specimen.

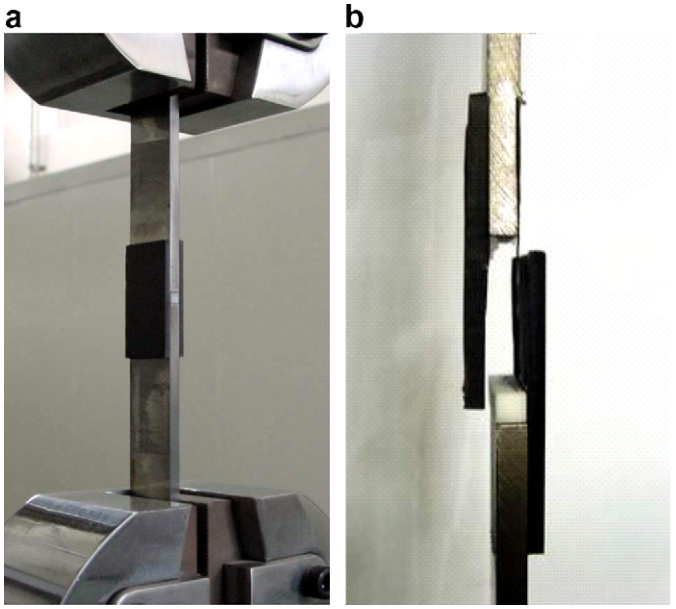

Fig. 11. Tensile test of the double lap joint: (a) apparatus and (b) fractured specimen.

fracture stress. This brittle failure behavior validates the stress intensity based linear elastic fracture mechanics characterization. Fig. 13 shows a fractured surface and its magnified view from the optical microscope. From the investigation of the fractured surface, we conclude that the failure mode of the co-cured lap joints is a partial cohesive failure within the epoxy resin layer and at the interface. As shown in Fig. 13, we can see epoxy resin all over the fractured steel surface with locally remaining carbon fibers. This means that interfacial

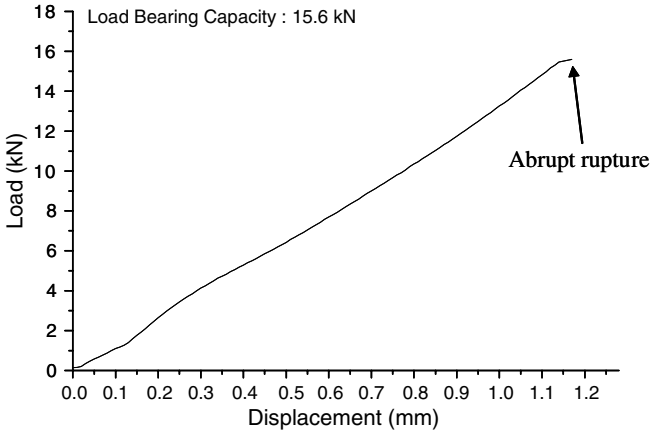

Fig. 12. Brittle behavior of the co-cured double lap joint.

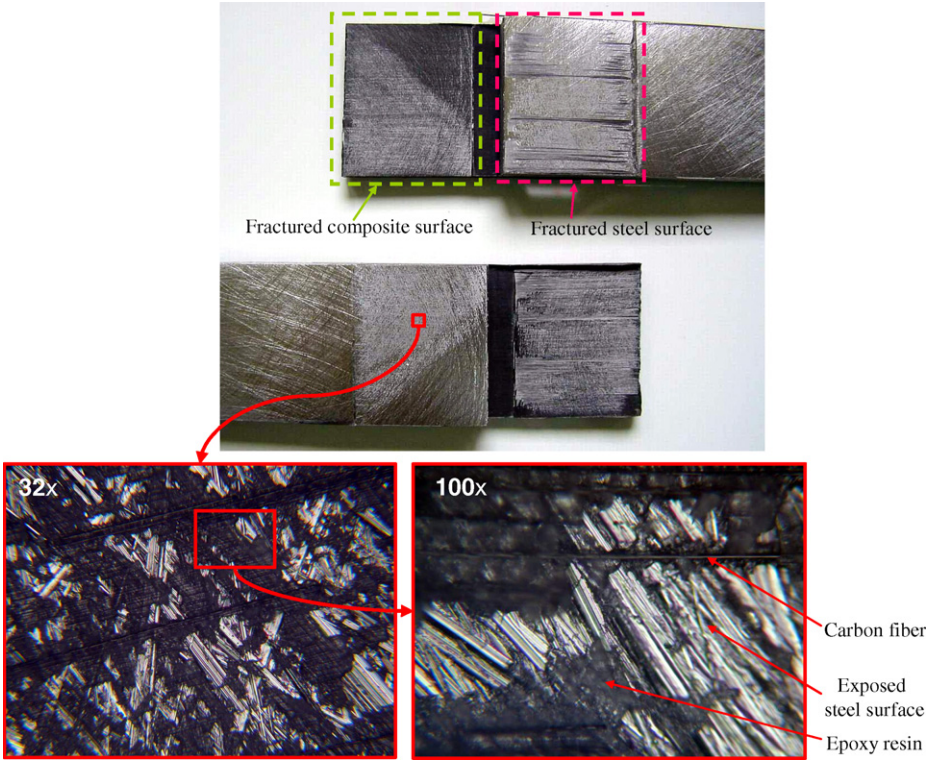

Fig. 13. Fractured surface of a steel adherend.

adhesion strength determines the load bearing capacity of the co-cured double lap joint. By inspecting the fractured surface, it is also found that a crack initiates at the inner composite/steel interface corner and propagates within the resin layer or along the interface. After crack initiation, it takes little time for its propagation until final rupture. Due to this unstable crack propagation behavior after its initiation, we can correlate both crack initiation and final fracture with critical stress intensities. Fig. 14 shows a magnified view of the steel/composite interface. It can be seen that there is no defect or crack along the interface shown at a micrometer scale. This means that the stress intensity of wedge-shaped bi-material interface corner without a crack is a valid approach. Load bearing capacities of double lap joints with varying bond lengths are listed in Table 3.

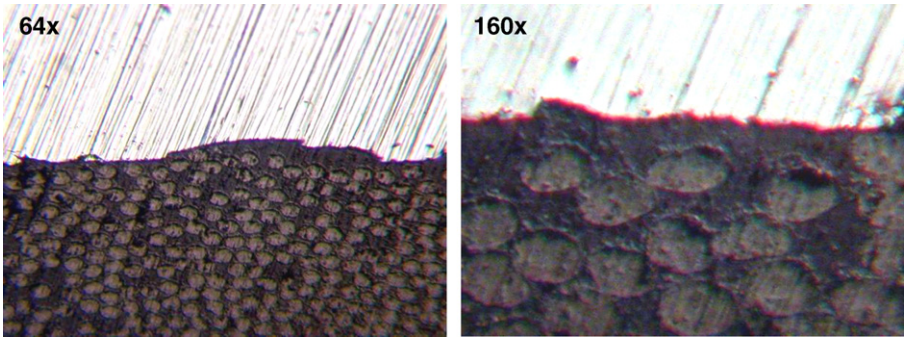

Fig. 14. Composite/steel interface observation using an optical microscope.

Table 3
Critical stress intensities in mixed mode

Bond length (mm)	Load bearing capacity (kN)	K_{IC}^{N} (MPa mm$^{0.487}$)	K_{IIC}^{N} (MPa mm$^{0.379}$)
10	9	−5.0	79.2
20	14	−7.2	104.3
30	17.8	−8.2	118.2

6. Finite element analysis results

To obtain stress and displacement fields for the double lap joint specimen, a two-dimensional finite element analysis considering both thermal residual stresses and mechanical loading was performed using the commercial software package ABAQUS (ABAQUS, 2004). Fig. 15 shows the finite element model and interfacial stress distributions (σ_{22}, τ_{12}) of the co-cured double lap joint. Only one quarter of the double lap joint specimen is modeled due to symmetry of the joint configuration. The interface between composite and steel adherends is idealized as perfect bonding. Technically, the two adherends share the same nodal points along the interface. The finite element model consists of 15,984 eight-node plane strain elements. The mesh around the interface corner tip is refined to consider singularity, as shown in Fig. 16. Quarter point singular elements are constructed around the corner tip to improve analysis efficiency. Thermal and mechanical loads are applied sequentially. Due to the misfit of thermal expansion coefficients of the two adherends, residual stresses, which are shown in Fig. 17, develop along the interface after the co-curing process. In addition, the stresses from the sequentially applied mechanical loads are superposed to the residual stresses, which are shown in Fig. 18. Sharp risings of stresses are shown at both corner tips of the interface. It is found that though mode II is more severe than mode I, mode I singularity surely exists in the co-cured double lap joint under tensile loading, because the normal stress component, σ_{22}, as well as shear stress components, τ_{12}, diverges to infinity at the interface corner. Interestingly, the interfacial normal stress field, σ_{22}, developed near the interface corner shows negative singularity, i.e., diverges to negative infinity. These compressive normal stresses developed near the wedge tip can increase the interfacial strength by constraining crack initiation and propagation.

To identify the availability of stress intensities as a design parameter, double lap joints are analyzed with varying bond lengths. Critical stress intensities are obtained from stress intensities at the failure load for each 10-, 20-, and 30-mm bond length specimen. To consider the mode mixity, critical stress intensities are plotted on the $K_{\mathrm{I}}^{n} - K_{\mathrm{II}}^{n}$ plane describing fracture initiation criterion in the next chapter.

7. Calculation of stress intensities with *H*-integral and the failure criterion

The path-independent *H*-integral is based on the application of Betti's reciprocal work theorem to the interface corner geometry. Betti's reciprocal work theorem is based on two sets of elastic fields: the actual and the complementary. In the absence of body forces, the *H*-integral takes the form (see Fig. 19):

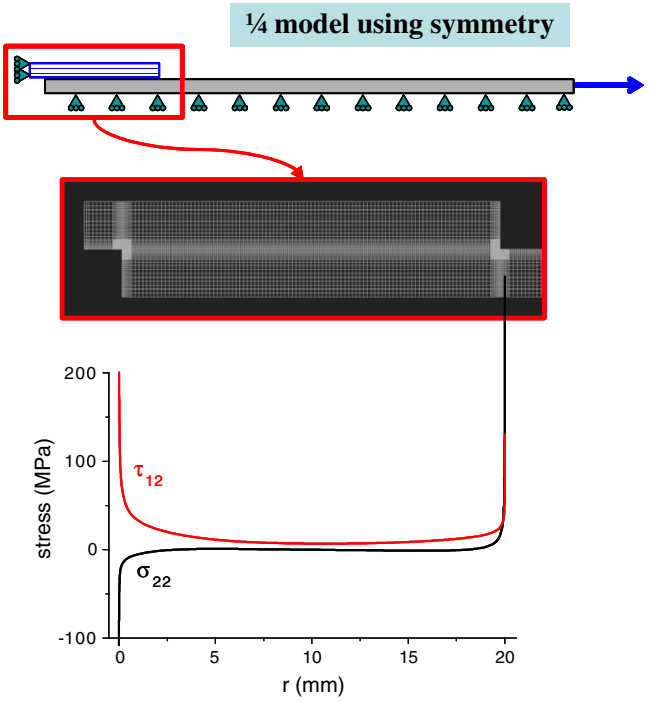

Fig. 15. Stress distributions along the interface obtained from finite element method.

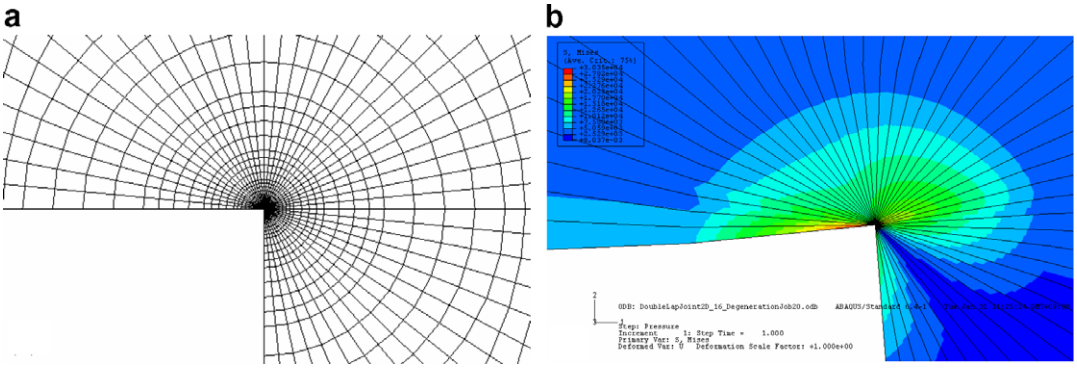

Fig. 16. The finite element mesh and obtained stress distribution at the interface corner tip: (a) refined mesh and (b) singular stress field.

$$H = \int_{\Gamma} (\sigma_{ij} u_i^* - \sigma_{ij}^* u_i) n_j \mathrm{d}s. \tag{15}$$

Here σ_{ij} and u_i are the actual stresses and displacements. These can be obtained practically from the finite element method or the boundary element analysis. σ_{ij}^* and u_i^* are the complementary fields, and n_j are components of outward unit vector, normal to the counter-clockwise contour Γ. Complementary fields can be any fields that satisfy the same equilibrium and constitutive relations as the actual fields The value of H taken along any closed contour not containing a singularity is zero. Under the boundary conditions of traction-free interface corner flanks and choosing a complementary field that satisfies the same boundary conditions as the actual field, H-integral along the corner flanks becomes zero. Therefore the path independency of H-integral along arbitrary contours from lower to upper flanks is maintained. Since the H-value is a constant that is determined by the singular stress field we can scale the value of H-integral as the stress intensities by choosing

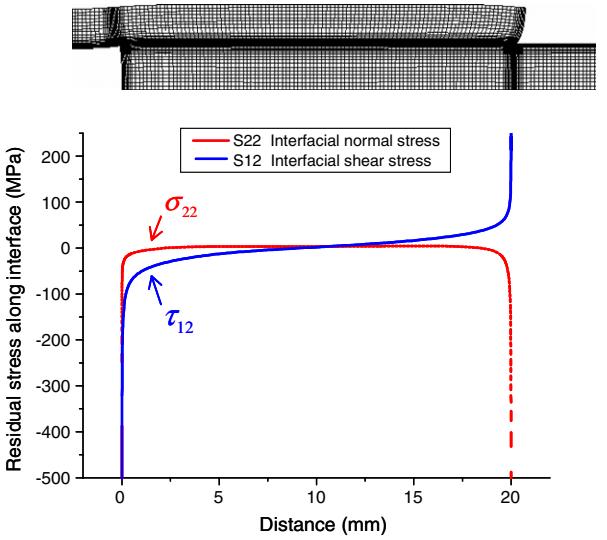

Fig. 17. Thermal residual stress distributions along the interface.

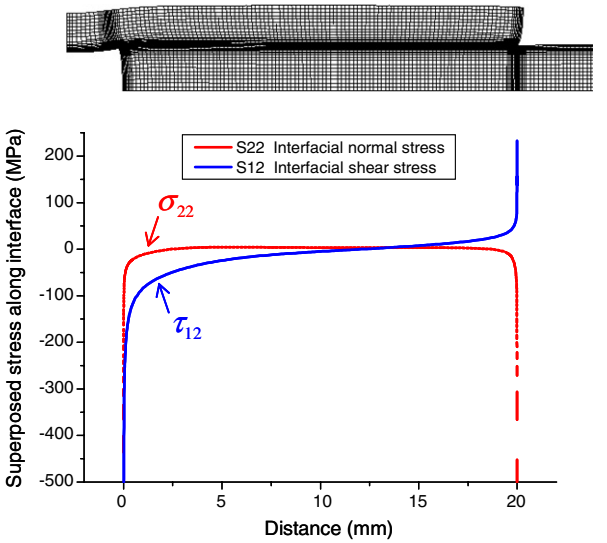

Fig. 18. Mechanical load superposed stress distributions along the interface.

a special complementary field. To determine K_{I}^{n}, we evaluate H using the mode I complementary field, and to determine K_{I}^{n}, we evaluate H using the mode II complementary field. It is well known that if the eigenvalue solution of given elasticity problem is λ, then $-\lambda$ can also be a solution satisfying the same equilibrium and boundary conditions although it is not physically admissible. By taking the complementary field as the eigenvector state corresponding to $\lambda^{*} = -\lambda_{\mathrm{I}}$, i.e., the mode I complementary field, we can scale the H value as K_{I}^{n}. In the same way, using the mode II complementary field obtained by $\lambda^{*} = -\lambda_{\mathrm{II}}$, we can determine K_{II}^{n}. The verification detail of how these choice of complementary fields can make H-integral values as stress intensities is shown in Hong and Stern (1978) for crack problems and Carpenter (1984) and Carpenter and Byers (1987) for wedge problems.

The complementary solution is obtained in the same way as the asymptotic solution. That is, we choose the complementary solution to be given by Eqs. (13) and (14) with eigenvalue $\lambda^{*} = -\lambda$. For calculating K_{I}^{n}, we choose complementary fields, as follows:

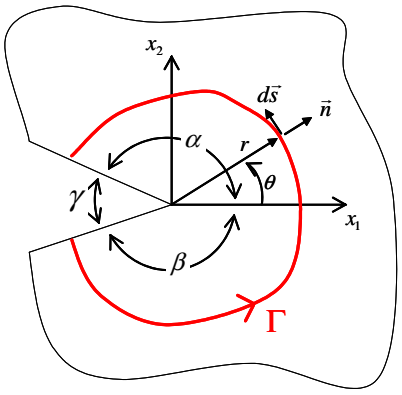

Fig. 19. A contour path for H-integration.

$$\begin{aligned}\sigma_{ij}^{\mathrm{IM}^*} &= K_{\mathrm{I}}^{n^*} r^{-\lambda_{\mathrm{I}}-1} f_{ij}^{\mathrm{IM}^*}(\theta)\\ u_i^{\mathrm{IM}^*} &= K_{\mathrm{I}}^{n^*} r^{-\lambda_{\mathrm{I}}} g_i^{\mathrm{IM}^*}(\theta).\end{aligned} \tag{16}$$

In the case of K_{II}^{n}, we choose complementary fields, as follows:

$$\begin{aligned}\sigma_{ij}^{\mathrm{IIM}^*} &= K_{\mathrm{II}}^{n^*} r^{-\lambda_{\mathrm{II}}-1} f_{ij}^{\mathrm{IIM}^*}(\theta)\\ u_i^{\mathrm{IIM}^*} &= K_{\mathrm{II}}^{n^*} r^{-\lambda_{\mathrm{II}}} g_i^{\mathrm{IIM}^*}(\theta).\end{aligned} \tag{17}$$

For both modes, $f_{ij}^{*}(\theta)$ and $g_i^{*}(\theta)$ are determined in the same way $f_{ij}(\theta)$ and $g_i(\theta)$ were determined. The only unknowns in Eqs. (16) and (17) are then the mode I and mode II complementary scaling factors, $K_{\mathrm{I}}^{n^*}$ and $K_{\mathrm{II}}^{n^*}$. For mode I loading of the interface corner, we obtain the scaling factor $K_{\mathrm{I}}^{n^*}$ by setting $H = H_{\mathrm{I}} = K_{\mathrm{I}}^{n}$ and evaluating the integral in Eq. (15) along an arc contour with a distance r from the tip of the interface corner that extends from the lower face to the upper face as shown in Fig. 19, using the asymptotic solution for σ_{ij} and u_i of Eq. (14). Explicitly, this is written in polar coordinates as (Sinclair, 1985; Labossiere and Dunn, 1999)

$$H = H_{\mathrm{I}} = \int_{-\beta}^{\alpha} (\sigma_{rr} u_r^{\mathrm{I}^*} + \sigma_{r\theta} u_\theta^{\mathrm{I}^*} - \sigma_{rr}^{\mathrm{I}^*} u_r - \sigma_{r\theta}^{\mathrm{I}^*} u_\theta) r \mathrm{d}\theta = \int_{-\beta}^{\alpha} \left(\sum_{i,j=1}^{2} n_i \sigma_{ij} u_j^{\mathrm{I}^*} - n_i \sigma_{ij}^{\mathrm{I}^*} u_j \right) r \mathrm{d}\theta = K_{\mathrm{I}}^{n}, \tag{18}$$

where $n_1 = \cos\theta$ and $n_2 = \sin\theta$. We can obtain the mode I scaling factor $K_{\mathrm{I}}^{n^*}$ as follows:

$$K_{\mathrm{I}}^{n^*} = 1 \Bigg/ \left\{ \int_{-\beta}^{\alpha} \left(\sum_{i,j=1}^{2} n_i f_{ij}^{\mathrm{I}} g_j^{\mathrm{I}^*} - n_i f_{ij}^{\mathrm{I}^*} g_j^{I} \right) \mathrm{d}\theta \right\}. \tag{19}$$

The same procedure is used to obtain the mode II scaling factor $K_{\mathrm{II}}^{n^*}$ by setting $H = H_{\mathrm{II}} = K_{\mathrm{II}}^{n}$ and evaluating the integral in Eq. (18). The mode II scaling factor $K_{\mathrm{II}}^{n^*}$ is obtained as follows:

$$K_{\mathrm{II}}^{n^*} = 1 \Bigg/ \left\{ \int_{-\beta}^{\alpha} \left(\sum_{i,j=1}^{2} n_i f_{ij}^{\mathrm{II}} g_j^{\mathrm{II}^*} - n_i f_{ij}^{\mathrm{II}^*} g_j^{\mathrm{II}} \right) \mathrm{d}\theta \right\}. \tag{20}$$

With this choice of complementary fields, the H-integral can be calculated for an arbitrary bi-material interface corner by computing real stress and displacement fields using the finite element method. Both thermal and mechanical loadings can be considered easily in the finite element analysis (see Figs. 17 and 18). Some circular contours are taken along the nodal points to retrieve stress and displacement data from the finite element analysis result, as shown in Fig. 20. Finally, we obtain the stress intensities as follows:

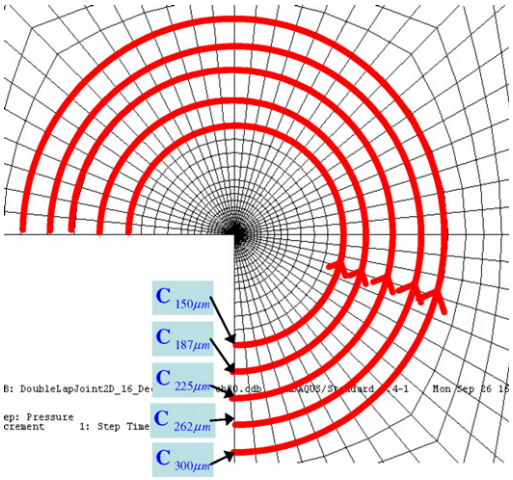

Fig. 20. Contour integration paths passing through nodal points.

$$K_{\mathrm{I}}^{n} = \int_{-\beta}^{\alpha} \left(\sum_{i,j=1}^{2} n_j \sigma_{ij} u_i^{I^*} - n_j \sigma_{ij}^{I^*} u_i \right) r \mathrm{d}\theta$$
$$K_{\mathrm{II}}^{n} = \int_{-\beta}^{\alpha} \left(\sum_{i,j=1}^{2} n_i \sigma_{ij} u_j^{\mathrm{II}^*} - n_i \sigma_{ij}^{\mathrm{II}^*} u_j \right) r \mathrm{d}\theta, \tag{21}$$

where $\sigma_{ij}^{\mathrm{I}^*}$, $u_i^{\mathrm{I}^*}$, $\sigma_{ij}^{\mathrm{II}^*}$, and $u_i^{\mathrm{II}^*}$ are calculated from Eqs. (16) and (17). σ_{ij} and u_i are obtained from the finite element analysis. The numerical computation of H-integral was carried out using stress and displacement components at nodal points along the contour and analytical complementary fields corresponding to these points. Fig. 21 shows H-integration results with respect to different radii of contours. As the contour radii become larger, the H value converges. For the double lap joint specimen with a 20 mm bond length, the critical stress intensities are calculated as -7.2 MPa mm$^{0.487}$ for K_{Ic}^{n} and 104.3 MPa mm$^{0.379}$ for K_{IIc}^{n}. Critical stress intensities with respect to different bond lengths of double lap joints are summed up in Table 3. As mentioned earlier, compressive interfacial stress near the interface corner shows singular behavior, and the critical mode I stress intensity, K_{Ic}^{n} is determined as a negative value. Former works (Glushkov et al., 2000; Banks-Sills and Ishbir, 2004) also showed negative mode I stress intensities for wedge-shaped bi-material joints under thermal loading. Negative singular behavior caused by compressive interfacial stress distribution near the wedge tip increases the interfacial strength of bonded joints, because compressive stresses prohibit crack initiation and propagation.

The calculated stress intensities complete the asymptotic fields of Eq. (13), and the asymptotic analysis result is compared with the finite element analysis result, as shown in Fig. 22. In Fig. 22, stresses along the interface are plotted as a function of r, the distance from the wedge tip. The good agreement between the asymptotic solution result (represented by the line) and the FEM result (represented by the dots) verifies that the asymptotic solutions are correct. The small discrepancy between them comes from the fact that we used only singular terms in describing the stress states.

Table 3 and its plot on the $K_{\mathrm{I}}^{n} - K_{\mathrm{II}}^{n}$ plane in Fig. 23 show that as the mode I stress intensity becomes larger in the negative, it needs a higher mode II stress intensity to bring about the fracture of the joint. This means that a different bond length changes the critical stress intensity pair, (K_{Ic}^{n}, K_{IIc}^{n}), in a mixed mode condition at the interface corner. In other words, single pair of critical stress intensities is not sufficient to predict the failure of the joint. We plotted three critical stress intensity points on the plane and linearly interpolated and extrapolated the points to make a fracture onset criterion of co-cured double lap joints. The fracture criterion based on the stress intensity is determined as

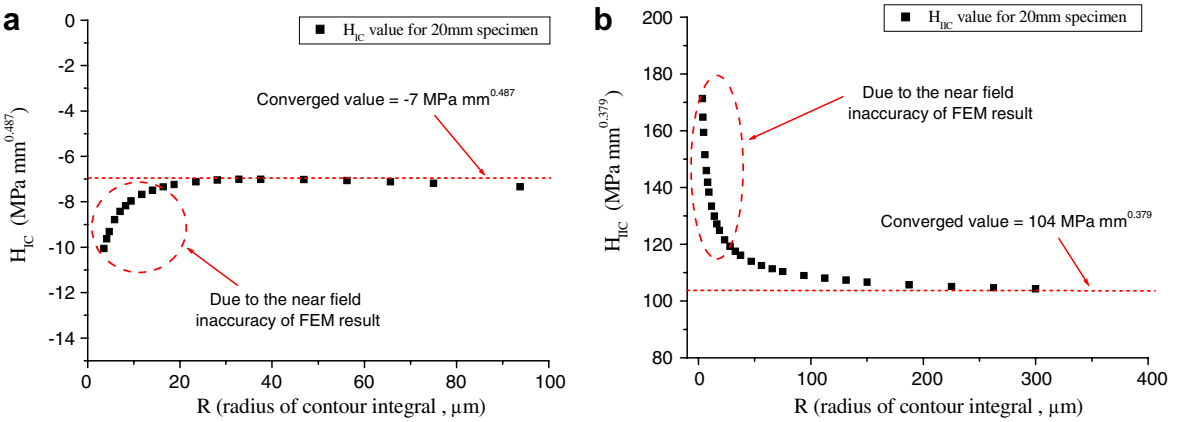

Fig. 21. *H*-integration values with varying contour paths: (a) for mode I and (b) for mode II.

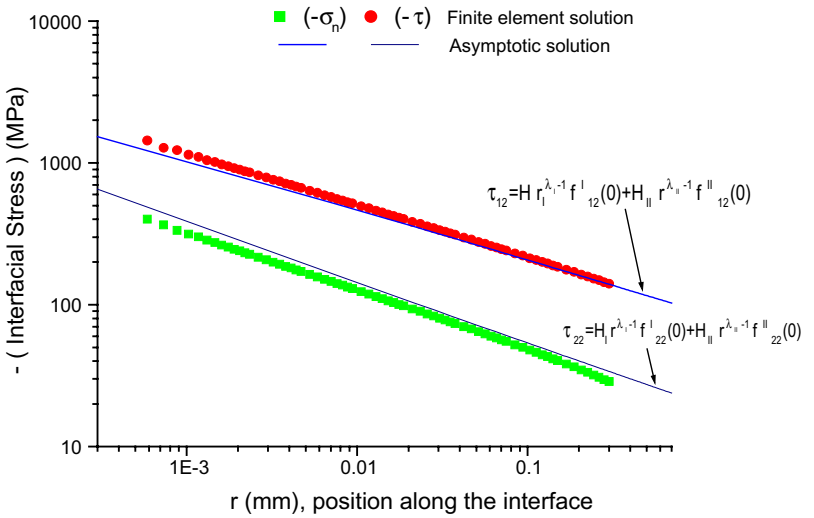

Fig. 22. Comparison of the asymptotic stress fields with FEM results.

$$f = \frac{K_{\mathrm{I}}^{n}}{K_{\mathrm{Ic}}^{n}} + \frac{K_{\mathrm{II}}^{n}}{K_{\mathrm{IIc}}^{n}} = \frac{K_{\mathrm{I}}^{n}}{1.6} + \frac{K_{\mathrm{II}}^{n}}{19.4} \geqslant 1, \tag{22}$$

where $K_{\mathrm{Ic}}^{n} = 1.6\ \mathrm{MPa\ mm}^{0.487}$ and $K_{\mathrm{IIc}}^{n} = 19.4\ \mathrm{MPa\ mm}^{0.379}$ are the critical stress intensities of pure modes I and II, respectively. They are intercepts of the extrapolated line with abscissa and ordinate in Fig. 23. Once $f \geqslant 1$, a crack initiates at the interface corner and grows rapidly to rupture in the case of co-cured double lap joints with the anisotropic/isotropic bi-material. This failure criterion can be used regardless of remote boundary and loading conditions of the joint.

8. Conclusion

In this paper, a fracture mechanics approach was presented to characterize fracture onset at the anisotropic/isotropic interface corner based on stress intensities, K_{I}^{n} and K_{II}^{n}. Using the expanded Stroh formalism, we formulated an anisotropic/isotropic interface corner problem with a wedge and obtained an asymptotic solution that describes the stress distribution near the interface corner. Specifically, the conservative *H*-contour integral method was applied to obtain stress intensities at the interface corner of the

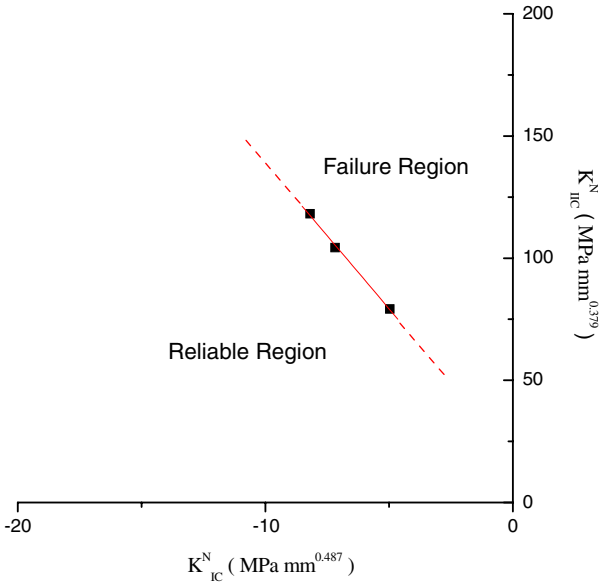

Fig. 23. Stress intensity based mixed mode failure criterion.

double lap joint under tensile loading condition. Two singular terms were found from the eigenfunction expansion series to approximate the stress and displacement fields at the interface corner. Stress singularity orders, i.e., $\lambda_1 = 0.513$ and $\lambda_2 = 0.621$ were weaker than those of crack problems, i.e., $\lambda = 0.5$. Although double lap joints are mostly under the second deformation mode, i.e., the second singular term mode, stress intensities of the two terms, K_{I}^n and K_{II}^n played important roles in the failure of double lap joints. A failure criterion of the composite/steel co-cured double lap joint was acquired by experimentally determining the critical stress intensities. The mixed-mode failure criterion on the $K_{\mathrm{I}}^n - K_{\mathrm{II}}^n$ plane can allow us to predict the failure of lap joints regardless of overall shape and loading conditions of bonded joints as long as the same asymptotic boundary conditions, i.e. half plane (anisotropic)/quarter plane (isotropic) bi-material interface corner are present. In conclusion, the proposed method for obtaining stress intensities at the interface corner of an anisotropic/isotropic bi-material can be used to estimate the load bearing capacity of bonded joints in a unified way and regardless of the adherend materials and geometry whereas stress based analysis methods can not.

References

ABAQUS/Standard User's Manual, 2004. Hibbitt, Karlsson, and Sorensen, Inc.

Adams, R.D., 1987. Theoretical stress analysis of adhesively bonded joints. In: Matthews, F.L. (Ed.), Joining Fiber Reinforced Plastics. Elsevier, London.

Akisanya, A.R., Fleck, N.A., 1997. Interfacial cracking from the free-edge of a long bi-material strip. Int. J. Solids Struct. 33, 1645–1665.

ASTM D3528-96 (Reapproved 2002). Standard test method for strength properties of double lap shear adhesive joints by tension loading.

Banks-Sills, L., Ishbir, C., 2004. A conservative line integral for bimaterial notches subjected to thermal stresses. Int. J. Numer. Meth. Eng. 60, 1075–1102.

Bogy, D.B., 1971. Two edge-bonded elastic wedges of different materials and wedge angles under surface tractions. Trans. ASME. J. Appl. Mech. 38, 377–386.

Carpenter, W.C., 1984. Calculation of fracture mechanics parameters for a general corner. Int. J. Fract. 24, 45–58.

Carpenter, W.C., Byers, C., 1987. A path independent integral for computing stress intensities for v-notched cracks in a bi-material. Int. J. Fract. 35, 245–268.

Cho, Y.J., Beom, H.G., Earmme, Y.Y., 1994. Application of a conservation integral to an interface crack interacting with singularities. Int. J. Fract. 65, 63–73.

Choi, S.T., Shin, H., Earmme, Y.Y., 2003. On the unified approach to anisotropic and isotropic elasticity for singularity, interface and crack in dissimilar media. Int. J. Solids Struct. 40, 1411–1431.

Chue, C.H., Liu, C.I., 2002. Stress singularities in a bimaterial anisotropic wedge with arbitrary fiber orientation. Comp. Struct. 58, 49–56.
Dempsy, J.P., 1981. The wedge subjected to tractions: a paradox resolved. J. Elasticity 11, 1–10.
Dempsy, J.P., Sinclair, G.B., 1979. On the stress singularities in the plane elasticity of the composite wedge. J. Elasticity 9, 373–391.
Dempsy, J.P., Sinclair, G.B., 1981. On the singular behavior at the vertex of a bimaterial wedge. J. Elasticity 11, 317–327.
England, A.H., 1971. On stress singularities in linear elasticity. Int. J. Eng. Sci. 9, 571–585.
Eshelby, J.D., Read, W.T., Shockley, W., 1953. Anisotropic elasticity with applications to dislocation theory. Acta Metall. 1, 251–259.
Glushkov, E.V., Glushkova, N.V., Munz, D., Yang, Y.Y., 2000. Analytical solution for bonded wedges under thermal stresses. Int. J. Fract. 106, 321–339.
Hong, C., Stern, M., 1978. The computation of stress intensity factors in dissimilar materials. J. Elasticity 8, 21–34.
Karp, S., Karal, F., 1962. The elastic-field behavior in the neighborhood of a crack of arbitrary angle. Commun. Pur. Appl. Math. 15, 413–421.
Labossiere, P., Dunn, M., 1999. Stress intensities at interface corners in anisotropic bimaterials. Eng. Frac. Mech. 62, 555–575.
Labossiere, P., Dunn, M., Cunningham, S., 2002. Application of biomaterial interface corner failure mechanics to silicon/glass anodic bonds. J. Mech. Phys. Solids 50, 405–433.
Lekhnitskii, S.G., 1963. Theory of Elasticity of an Anisotropic Body. Holden-Day Inc., San Francisco.
Muskhelishvili, N.I., 1953. Some Basic Problems of the Mathematical Theory of Elasticity. Noordhoff, Groningen.
Reedy, E.D., Guess, T.R., 1993. Comparison of butt tensile strength data with interface corner stress intensity factor prediction. Int. J. Solids Struct. 30, 2929–2936.
Reedy, E.D., Guess, T.R., 1997. Interface corner failure analysis of joint strength: effect of adherend stiffness. Int. J. Fract. 88, 304–305.
Sinclair, G.B., 1985. A remark on the determination of mode I and mode II stress intensity factors for sharp re-entrant corners. Int. J. Fract. 27, R81–R85.
Sinclair, G.B., Mullan, D., 1982. A simple yet accurate finite element procedure for computing stress intensity factors. Int. J. Numer. Meth. Eng. 18, 1587–1600.
Sinclair, G.B., Okajima, M., Griffin, J.H., 1984. Path independent integral for computing stress intensity factors at sharp notches in elastic strips. Int. J. Numer. Meth. Eng. 20, 999–1008.
Stern, M., 1979. The numerical calculation of thermally induced stress intensity factors. J. Elasticity 9, 91–95.
Stern, M., Soni, M.L., 1976. On the computation of stress intensities at fixed-free corners. Int. J. Solids Struct. 12, 331–337.
Stern, M., Becker, E.B., Dunham, R.S., 1976. A contour integral computation of mixed mode stress intensity factors. Int. J. Fract. 12, 359–368.
Stroh, A.N., 1958. Dislocations and cracks in anisotropic elasticity. Phil. Mag. 3, 625–646.
Suo, Z., 1989. Singularities interacting with interfaces and cracks. Int. J. Solids Struct. 25, 1133–1142.
Suo, Z., 1990. Singularities, interfaces and cracks in dissimilar anisotropic media. Proc. R. Soc. Lond. A427, 331–358.
Ting, T.C.T., 1982. Effects of change of reference coordinates on the stress analyses of anisotropic elastic materials. Int. J. Solids Struct. 18, 139–152.
Ting, T.C.T., 1986. Explicit solution and invariance of the singularities at an interface crack in anisotropic composites. Int. J. Solids Struct. 22, 965–983.
Ting, T.C.T., 1996. Anisotropic Elasticity: Theory and Applications. Oxford University Press, New York.
Ting, T.C.T., Chou, S.C., 1981. Edge singularities in anisotropic composites. Int. J. Solids Struct. 17, 1057–1068.
Tong, L., 1998. Failure of adhesive-bonded composite single lap joints with embedded cracks. AIAA J. 36, 448–456.
Williams, M.L., 1952. Stress singularities resulting from various boundary conditions in angular corners of plates in extension. J. Appl. Mech. 19, 526–528.
Williams, M.L., 1957. On the stress distribution at the base of a stationary crack. J. Appl. Mech. 24, 109–114.